Plasmon-in-A-Box: On the Physical Nature of Few-Carrier Plasmon Resonances

ARTICLE *in* JOURNAL OF PHYSICAL CHEMISTRY LETTERS · AUGUST 2014

Impact Factor: 7.46 · DOI: 10.1021/jz501456t

1 AUTHOR:

Prashant K Jain
University of Illinois, Urbana-Champaign
63 PUBLICATIONS **9,022** CITATIONS

SEE PROFILE

THE JOURNAL OF PHYSICAL CHEMISTRY Letters

Letter

pubs.acs.org/JPCL

Plasmon-in-a-Box: On the Physical Nature of Few-Carrier Plasmon Resonances

Prashant K. Jain*

Department of Chemistry and Materials Research Lab, University of Illinois Urbana−Champaign, Urbana, Illinois 61801, United States

Supporting Information

ABSTRACT: Recent demonstrations in doped semiconductor nanocrystals establish that a plasmon resonance can be sustained by a handful of charge carriers, much smaller in number than conventionally thought. This finding raises questions about the physical nature of such a collective resonance, a fundamental question in condensed matter and many-body physics, which the author addresses here by means of a plasmon-in-a-box model. A small number of carriers confined within a nanocrystal exhibit multiple transitions of individual carriers between quantized states. However, as carriers are progressively added, spectral lines associated with single-carrier excitations evolve into a band representing a collective resonance. This evolution is gradual, and it involves an intermediate regime where single-carrier excitations and few-carrier collective excitations coexist, until, at high carrier numbers, a purely classical collective resonance involving all carriers in the nanocrystal is sustained. The author finds that the emergence of the plasmon resonance is a density-driven transition; at high enough carrier densities, the Coulomb repulsion between carriers becomes strong enough to allow individual carriers to overcome their confinement to the nanocrystal lattice and to participate in a collective excitation within the mean Coulomb field of other carriers. The findings represent deeper insight into the physical picture of a plasmon resonance and serve as a potential design guide for nanoscale optoelectronic components and photocatalytic plasmonic clusters.

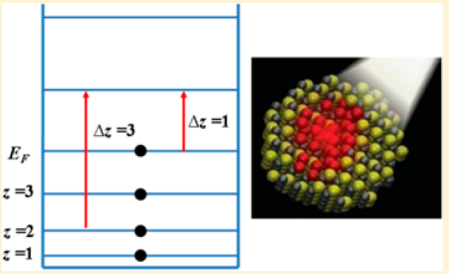

SECTION: Plasmonics, Optical Materials, and Hard Matter

Plasmon resonances[1−7]—collective electronic excitations that give rise to strong light−matter interactions—have been studied in metallic clusters, nanoparticles, and nanostructures since the time of Michael Faraday.[8] Over the decades of work in this field, it had become natural to associate plasmon resonances with electron-dense metals. Only more recently, plasmon resonances are being recognized to be ubiquitous, as exemplified by the induction of such resonances via free-carrier doping in nanostructures of semiconductors and oxides.[9−22]

Due to the long-held association of plasmons with electron-dense metals, conventional wisdom has been that rather large numbers of carriers are required for a plasmon resonance. This notion had to be revised when the author's laboratory demonstrated in photodoped ZnO nanocrystals that a collection of as few as four electrons can display a plasmon resonance-like absorption,[19] as also shown subsequently by Gamelin and Massiello.[21] The finding of a plasmon resonance-like absorption sustained by a handful of charge carriers raises a number of crucial questions,[22] which are addressed here:

(a) Plasmon resonances of semiconductor nanocrystals lie in the infrared region. In the past, infrared spectral bands arising from the addition of carriers to the conduction band of a semiconductor nanocrystal have been assigned to intraband excitations of carriers.[23] Can one make a distinction between such intraband excitations and a plasmon resonance?

(b) How small of a charge carrier collection can support a plasmon resonance? What are the physical requirements for setting up such a collective excitation? These questions are central to the understanding of the fundamental nature of a plasmon resonance, whether in a metal, a semiconductor, or any arbitrary solid.

(c) Are few-carrier plasmon resonances different in nature from those exhibited in electron-dense metals where a huge number of carriers are involved?

(d) What is the influence of carrier confinement or the bound nature of carriers on the nature of collective excitation?

(e) How does a collective excitation emerge from the response of individual carriers?[24]

As the subsequent discussion will show, all of these questions are inter-related. Some of these questions have been encountered in the experimental and theoretical study of the size dependence of plasmon resonances, particularly in ultrasmall metallic clusters.[5,6,25−28] However, with these studies, a satisfactory resolution of the above questions has been difficult due to an inherent complication; with metals, a small number n of electrons can be achieved only in ultrasmall cluster sizes because $n = zN$, where N is the number of metal atoms in

Received: June 19, 2014
Accepted: August 22, 2014

   dx.doi.org/10.1021/jz501456t | J. Phys. Chem. Lett. 2014, 5, 3112−3119

a cluster and z is the number of valence electrons per metal atom. In such ultrasmall metal clusters, the electronic structure is significantly altered from that of the bulk solid. The electronic structure is characterized by molecular-like orbitals rather than electronic (conduction and valence) bands typical of solids, resulting in molecular-like absorption features like those seen in the optical spectrum of Au_{25}.[27] Studying the pure effect of the number of carriers or the carrier density on the nature of electronic excitations is therefore not possible in a metallic system; variations in the electronic structure with cluster size dominate the observed evolution of the spectral response.

A newfound opportunity for addressing the aforementioned questions is made available by plasmon resonant semiconductor nanocrystals. Unlike a metal, where carrier density is mostly invariable, the number of charge carriers in many semiconductors (e.g., copper sulfide, copper selenide, zinc oxide) can be systematically varied via doping,[10,12,29−31] without requiring alterations in the crystallite size and/or structure. In addition, the order-of-magnitude lower carrier densities of degenerately doped semiconductors[10] relative to those of metals allow one to achieve an extremely small number of carriers in crystallites large enough in size for the electronic band structure to be closer to that of a solid than that of a molecule. The latter was exploited in the experimental demonstration of a four-electron plasmon resonance in 3 nm ZnO nanocrystals.[19] Recent studies of few-carrier plasmons in semiconductor nanocrystals have thus brought several unresolved issues to the fore, motivated by which the author presents here a theoretical study of the nature of such collective resonances in nanosolids.

In particular, the author shows how a collective resonance develops gradually as charge carriers are systematically added to the empty band of a nanocrystal. The author finds that there is a low carrier density regime where quantum mechanical intraband excitations of individual carriers dominate, an intermediate regime where few-carrier collective excitations coexist with single-carrier excitations, and a high carrier density regime where a purely collective excitation of all charge carriers in the sea is sustained. Thus, the emergence of a plasmon resonance is a gradual density-driven transition akin to a gas-to-liquid transition. This classical plasmon regime is reached at carrier densities where the motion of carriers is purely dictated by Coulomb repulsion between carriers rather than the confinement of carriers to the lattice. These findings reveal the previously undescribed nature of a plasmon resonance and also elucidate its metamorphosis as a function of the number of charge carriers (n) involved in the excitation, the crystallite size (a), and the effective mass (m_{eff}) of the carrier.

Particle-in-a-Box Model. For a problem of this nature, it is clear that electronic structure theory can be quite powerful in providing detailed calculations. However, with the objective of providing the most intuitive understanding, the author employs a simple effective mass model of a doped nanocrystal in the form of charge carriers confined to a three-dimensional box of size a (see the Methods Section).[32] Using this model, the optical response of the nanocrystal is calculated as a function of the number n of added charge carriers. The calculated optical response of the nanocrystal in the form of an extinction spectrum is shown in Figure 1b. The author's method makes several approximations, which are listed in the Methods Section; however, these approximations do not affect the qualitative merit of the results that the author obtains. More

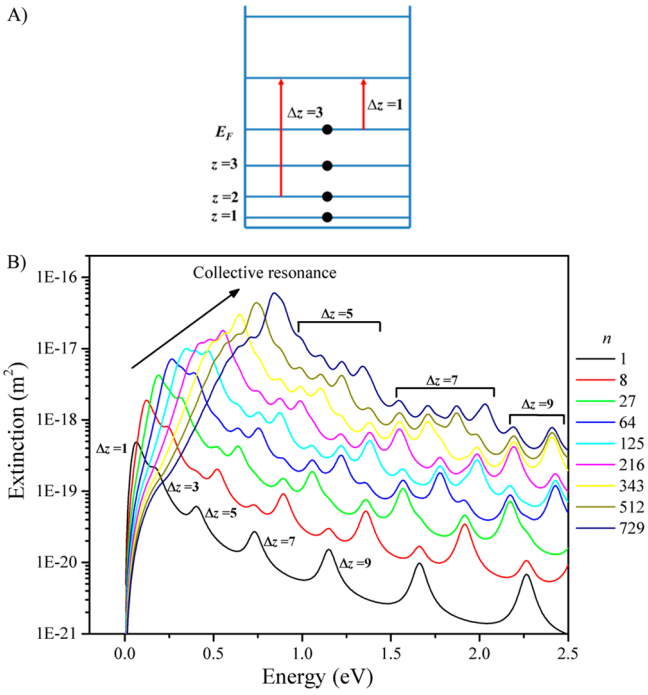

Figure 1. (A) The particle-in-a-box model used for calculation of the spectra. (B) Evolution of the optical spectrum of a nanocrystal as a function of the number of added charge carriers, showing the emergence of a collective resonance at a sufficiently high number of carriers. Calculations shown here were performed with a = 9 nm, $\gamma = 4\pi \times 10^{13}$ rad/s or 0.083 eV, ε_m = 2.1, ε_∞ = 3, m_{eff} = 0.4m_e, and a maximum carrier concentration of 10^{27} m^{-3} (n = 729), representative of a doped cuprous sulfide nanocrystal.[10]

rigorous calculations, with fewer approximations, should able to build upon the treatment here in order to provide more quantitative results for comparison with experiments. For instance, recent work, which appeared while the current Letter was in revision, utilizes time-dependent density functional theory to study similar phenomena.[33] The current work is focused on obtaining the most insight into the nature of emergence of a plasmon resonance. To ensure that the approximations made do not compromise the physical validity of the results, the author validates his method by comparing his theoretical calculations to experimental data for both a Au nanosphere and a doped $Cu_{2-x}Se$ (x = 0.2) nanocrystal (Supporting Information Figures S1 and S2).

Quantum Mechanical Intraband Transitions. Extra electrons (holes) added to the nanocrystal occupy discrete energy levels within the conduction (valence) band (see Figure 1a), raising the Fermi level ($E_F \alpha n^{2/3}$). A single charge carrier (n = 1) added occupies the lowest energy state with the quantum number z_F = 1. A progression of absorption peaks can be identified in the extinction spectrum (black curve).

These peaks correspond to quantum mechanical transitions of the added charge carrier from the Fermi level (z_F = 1) to unoccupied states ($z > z_F$) lying above the Fermi level. Individual peaks in the spectrum can be assigned, in progression from low to high energy, to quantum jumps of Δz = 1, 3, 5, 7, ... levels.

With multiple charge carriers added to the nanocrystal, one obtains, for each Δz, a manifold of spectral lines. Each spectral line represents single-carrier transitions emanating from occupied states within the Fermi sphere with a specific

dx.doi.org/10.1021/jz501456t | J. Phys. Chem. Lett. 2014, 5, 3112−3119

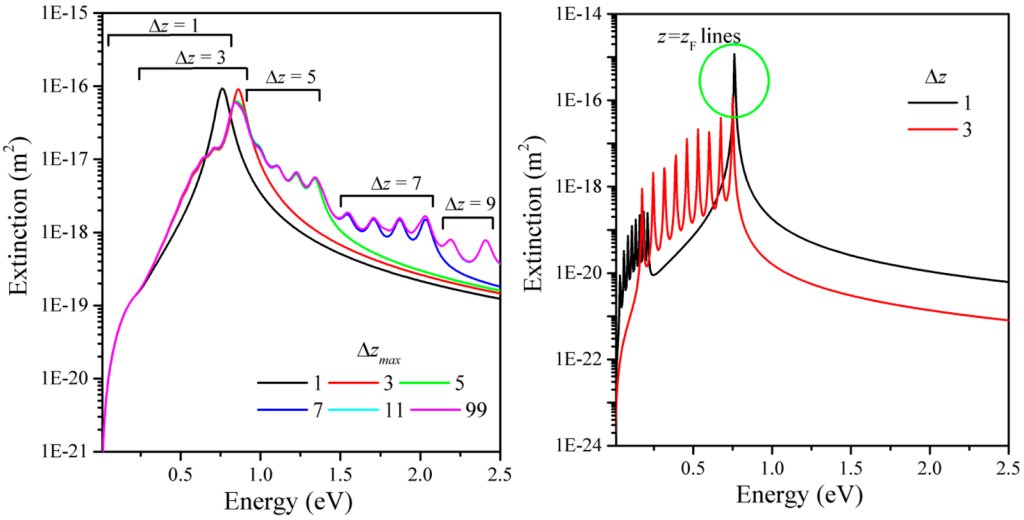

Figure 2. The emergent broad band is found to be composed mainly of quantum mechanical transitions of carriers from the highest occupied states ($z = z_F$) to unoccupied states directly above ($z = z_F + 1$). (A) All transitions corresponding to quantum jumps $\Delta z = 1, 3, 5, \ldots$ up to Δz_{max} were included in the calculation. Variation of Δz_{max} shows that the collective band can almost entirely be reproduced by including only the $\Delta z = 1$ and 3 transitions; higher-energy transitions modify this band only to a relatively small extent. (B) Fine structure of the $\Delta z = 1$ and 3 manifolds shows the contribution of transitions emanating from occupied states with quantum numbers $z = 1, 2, 3, \ldots, z_F$, seen as distinct lines ranging from low to high energy. The $z = z_F$ lines contribute most to the collective band. Spectra were calculated for a 9 nm size nanocrystal containing 729 carriers corresponding to $z_F = 9$ and a carrier density $\rho = 10^{27}$ m^{-3}. Values of other parameters were $\varepsilon_m = 2.1$, $\varepsilon_\infty = 3$, and $m_{eff} = 0.4m_e$. The value of γ was $4\pi \times 10^{13}$ rad/s for the spectrum in (A) and $0.2\pi \times 10^{13}$ rad/s for the fine-structure version in (B).

quantum number $z = 1, 2, 3, \ldots, z_F$. Thus, there are z_F spectral lines within each manifold. As carriers are added to the nanocrystal, the number of lines within a manifold increases as $z_F = n^{1/3}$, and distinct spectral lines begin to overlap.

Emergence of a Broad Band. At a large number of carriers (e.g., $n = 343$, yellow curve), one observes the emergence of a broad band enveloping several overlapping intraband transitions. This broad band blue shifts as more carriers are added to the nanocrystal, consistent with recent experiments on copper sulfide, copper selenide, and zinc oxide nanocrystals.[10,12,19,27] Further analysis (Figure 2) shows that this band is dominated by excitations of carriers between the highest occupied states (i.e., Fermi surface) along the z-axis to unoccupied states directly above. After all, these $z_F \rightarrow z_F + 1$ excitations constitute the strongest transitions, as expected from the oscillator strength ($A_{z,\Delta z}\Omega_{z,\Delta z}$, including the degeneracy factor)[34]

$$A_{z,\Delta z}\Omega_{z,\Delta z} = \frac{32}{\pi}\frac{z^2(z+\Delta z)^2}{\Delta z^2(2z+\Delta z)^2} \approx \frac{8}{\pi}\frac{z^2}{\Delta z^2} \tag{1}$$

The $z_F \rightarrow z_F + 3$ excitations, while relatively weaker, also contribute to the peak of this broad band (Figure 2a).

Assignment of the Emergent Band to a Collective Resonance. The author shows that this emergent band represents a collective excitation of carriers at the Fermi surface and is what evolves into the well-known plasmon resonance in the classical large carrier limit. With only one carrier ($n = 1$, $z_F = 1$), the dielectric function considering only the strongest $\Delta z = 1$ transitions is

$$\varepsilon(\omega) \approx \varepsilon_\infty + \frac{8e^2}{\pi\varepsilon_0 m_{eff} a^3}\left(\frac{1}{\omega_{1\rightarrow 2}^2 - \omega^2 - i\omega\gamma_{1\rightarrow 2}}\right) \tag{2}$$

representing simply the Lorentzian response due to a single-carrier intraband transition ($z = 1 \rightarrow 2$) of energy $\omega_{1\rightarrow 2}$ and line width $\gamma_{1\rightarrow 2}$. ε_∞ is the high-frequency dielectric constant. With additional carriers added to the nanocrystal ($n > 1$), the dielectric function

$$\varepsilon(\omega) \approx \varepsilon_\infty + \frac{8e^2}{\pi\varepsilon_0 m_{eff} a^3}\sum_{z}^{1,2,\ldots,z_F}\frac{z^2}{\omega_{z\rightarrow z+1}^2 - \omega^2 - i\omega\gamma_{z\rightarrow z+1}} \tag{3}$$

represents a combination of several intraband transitions that form the $\Delta z = 1$ manifold. In the limit of a large number of carriers ($z_F \gg 1$), the second term can be approximated as an integral

$$\varepsilon(\omega) \approx \varepsilon_\infty + \frac{8e^2}{\pi\varepsilon_0 m_{eff} a^3}\int_1^{z_F}\frac{z^2}{\omega_{z\rightarrow z+1}^2 - \omega^2 - i\omega\gamma_{z\rightarrow z+1}}\,dz \tag{4}$$

which further approximates to

$$\varepsilon(\omega) \approx \varepsilon_\infty - \frac{ne^2}{\varepsilon_0 m_{eff} a^3}\cdot\left(\frac{1}{\omega^2 - \omega_{qm1}^2 + i\omega\gamma_{qm1}}\right) \tag{5}$$

by recognizing ${z_F}^3 = n$, ${z_F}^3 \gg 1$ and considering only the strongest transitions that emanate from states at the Fermi surface ($z = z_F$). ω_{qm1} represents the energy of these $z_F \rightarrow z_F + 1$ transitions, and γ_{qm1} is their damping rate. The emergent term $ne^2/\varepsilon_0 m_{eff} a^3$ has units of ω^2 and is recognized to be the square of the bulk plasma frequency (ω_p^2) in the Drude model. Thus, one gets

$$\varepsilon(\omega) \approx \varepsilon_\infty - \frac{\omega_p^2}{\omega^2 - \omega_{qm1}^2 + i\omega\gamma_{qm1}} \tag{6}$$

which resembles the familiar Drude response for a free-carrier sea, with the exception of the ω_{qm1}^2 term, which can be thought of as a quantum mechanical correction to the free-carrier

dx.doi.org/10.1021/jz501456t | J. Phys. Chem. Lett. 2014, 5, 3112−3119

response resulting from single-carrier transitions excited at the Fermi surface. Equation 6 can be employed as the dielectric function for describing the collective resonances of confined or bound carriers. While eq 6 only considers $z_F \rightarrow z_F + 1$ intraband excitations, depending on the carrier density, higher-energy excitations ($\Delta z = 3, 5, \ldots$ and so on) need to be included in the quantum mechanical contribution, as will be discussed later.

From eq 6 and the Clausius–Mossotti dipolar polarizability for a nanostructure with a shape factor κ, the resonance condition is obtained as

$$\omega_r^2 = \underbrace{\omega_{qm1}^2}_{\text{QM single-carrier excitation}} + \underbrace{\frac{\omega_p^2}{\varepsilon_\infty + \kappa\varepsilon_m}}_{\text{Classical collective excitation}} \tag{7}$$

Equation 7 captures the nature of the gradual emergence of the plasmon resonance, resulting from the interplay of two distinct types of excitations, as carriers are added to the nanocrystal:

(a) In the limit of one carrier, the second term, which results from the mean Coulomb field setup by other oscillating carriers, is unimportant, and the resonance band is purely due to quantum mechanical intraband transitions of an individual carrier at the Fermi surface with $\omega_r = \omega_{qm1}$.

(b) With added carriers, the quantum mechanical transitions described by the first term persist; however, as carriers fill higher and higher z states, the transition energy ω_{qm1} increases as z_F or $n^{1/3}$. At the same time, the increased density of carriers (n/a^3) results in the strengthening of Coulomb repulsion between carriers, which can no longer be neglected. This Coulomb repulsion results in a modification of the transition energy of a carrier undergoing excitations at the Fermi surface. This positive correction to the transition energy is represented by the second term in eq 7.

(c) ω_p is a measure of the rate of Coulomb scattering events and goes as $n^{1/2}$. Thus, $\omega_p$increases more rapidly than ω_{qm1} as carriers are added to the nanocrystal. At some number of carriers, ω_p becomes larger than ω_{qm1}. This represents a situation where the Coulomb interactions are strong enough that it becomes difficult to excite carriers individually. Collective excitations of carriers at the Fermi surface become prevalent. These collective excitations are manifested in an emergent broad band (like the one in Figure 1b), the resonance energy of which is represented by the second term in eq 7, with the first term serving as a quantum mechanical correction due to the discrete nature of the energy states involved in the collective excitation. This positive energy correction is responsible for the collective resonance energy of 0.84 eV for $n = 729$ in Figure 1b, being blue shifted relative to the value of 0.69 eV expected from the classical Drude model.

(d) In the limit of a large number of carriers, $\omega_p \gg \omega_{qm1}$ and the quantum mechanical correction to the collective excitation energy can be neglected, and the result is a classical collective excitation of the entire sea of carriers set up in the mean Coulomb field. The resonance energy of this oscillation is given by

$$\omega_r = \sqrt{\frac{\omega_p^2}{\varepsilon_\infty + \kappa\varepsilon_m}} \tag{8}$$

which is the localized surface plasmon resonance energy expected from the classical Drude model.

What Are the Conditions for a Collective Resonance to Emerge? The emergence of the collective resonance can be thought of as a density-driven transition. In a nanocrystal with a carrier density $\rho = n/a^3$, a carrier at the surface experiences a Coulomb repulsion energy

$$E_{Coulomb} \approx \frac{\rho a^3 e^2}{4\pi\varepsilon_0 \cdot \left(\frac{a}{2}\right)} = \frac{\rho a^2 e^2}{2\pi\varepsilon_0} \tag{9}$$

where a is the nanocrystal size. At a high enough density of carriers, this Coulomb repulsion energy, which is proportional to ρ, can become much greater than the kinetic energy of a Fermi level carrier resulting from the confinement of the carrier to the lattice

$$E_{confinement} = \frac{h^2 {z_F}^2}{8 m_{eff} a^2} \tag{10}$$

Thus, this confinement energy is seen to be proportional to $(z_F/a)^2$ or $\rho^{2/3}$. Thus at high carrier densities, one gets

$$\frac{\rho a^2 e^2}{2\pi\varepsilon_0} \gg \frac{h^2 {z_F}^2}{8 m_{eff} a^2} \tag{11}$$

$$\sqrt{\frac{\rho e^2}{m_{eff}\varepsilon_0}} \gg \frac{1}{\sqrt{\pi}} \cdot \frac{2\pi h \cdot 2 z_F}{8 m_{eff} a^2} \tag{12}$$

which one recognizes to be approximately equivalent to

$$\omega_p \gg \omega_{qm1} \tag{13}$$

The density ρ_c at which ω_p begins to exceed the quantum mechanical transition frequency ω_{qm1} is given as

$$\rho_c^{1/3} = \left(\frac{\pi}{2a}\right)^2 \cdot \frac{4\pi\varepsilon_0 (h/2\pi)^2}{m_{eff} e^2} \tag{14}$$

where the second term on the right-hand side is recognized to be the Bohr radius a_H. Above this density, the motion of Fermi level carriers begins to be dictated by their Coulomb repulsion with other carriers rather than by their confinement to the lattice. Under these conditions, Fermi level carriers begin to experience collective motion set up by the Coulomb repulsion field. As the density is increased further beyond ρ_c, at some point, ω_p begins to exceed ω_{qm3}, the high-frequency edge of $\Delta z = 3$ transitions, and subsequently, ω_p exceeds ω_{qm5} and so on. Thus, as the carrier density increases, carriers deeper and deeper within the Fermi sphere can participate in the collective motion setup within the Coulomb mean field, until at $\rho \gg \rho_c$, all carriers of the sea are involved in a collective resonance. Thus, the emergence of the plasmon resonance occurs gradually as a function of increasing ρ, in the same vein as the density-driven transition of a gas to a liquid.

The greater the Coulomb repulsion energy felt by a carrier (as compared to its own kinetic energy), the stronger the coupling of the carrier to other carriers. ρ/ρ_c, which is the ratio of the Coulomb repulsion energy to the kinetic energy, can therefore be thought of as a coupling constant for the many-body interaction. The higher the value of ρ/ρ_c, the greater the range of intraband transitions ($\Delta z = 1, 3, 5, \ldots$, and so on) that contribute to the collective excitation band and the larger the fraction of carriers that participate in a collective excitation. In essence, a description of the optoelectronic properties of the

dx.doi.org/10.1021/jz501456t | J. Phys. Chem. Lett. 2014, 5, 3112–3119

system in terms of single-carrier states is appropriate only at a very low carrier density ρ, where carrier−carrier interactions are negligible. As the carrier density ρ increases, a many-body description is needed; two-carrier states, three carrier states, and so on become increasingly important. Eventually, in the classical limit, an n-particle collective state involving the entire Fermi sea of carriers is the most accurate description.

Effect of the Bound Nature of a Carrier. Carriers in a semiconductor experience significant localization as they are bound to the periodic potential of the lattice. This is phenomenologically represented by the effective mass of the carrier; a smaller effective mass (relative to the mass of a free electron m_e) implies a more strongly bound carrier because $E_{confinement} \propto 1/m_{eff}$. Equation 14 predicts that for the same carrier density, the propensity for exhibiting a collective carrier excitation is higher for less strongly bound carriers. In other words, the weaker confinement of the carrier can be readily overcome by carrier−carrier repulsion. Indeed, calculated optical spectra as a function of m_{eff} at the same carrier density of 10^{27} m^{-3} confirm this prediction (Figure 3). As m_{eff} is increased, the spectrum evolves from one dominated by discrete intraband excitations to one exhibiting a collective resonance band enveloping several such excitations (Figure 3a). With increasing m_{eff}, the collective resonance band frequency approaches the plasmon resonance frequency expected from the classical Drude model (Figure 3b). The quantum mechanical contribution to the collective resonance frequency decreases with increasing effective mass as $1/m_{eff}$ (Figure 3b, inset).

Effect of Size. A similar effect is expected from eq 14 as a function of increasing nanocrystal size. In a smaller nanocrystal, carriers are more confined ($E_{confinement} \propto 1/a^2$), and quantum mechanical transitions dominate the spectrum (Figure 4a). As the size is increased, at a fixed carrier density of 10^{27} m^{-3}, one sees the emergence of a collective excitation band. With increasing size, the quantum mechanical contribution to the collective resonance decreases, and the resonance frequency of the collective band approaches the classical Drude value in the asymptotic limit of large size (Figure 4b). The prediction of relatively blue-shifted resonances at small nanoparticle sizes is consistent with recent observations in ultrasmall Ag nanoparticles by Dionne and coworkers.[35,36] However, in its approach to the classical plasmon resonance frequency, the peak frequency exhibits an oscillatory behavior as a function of size. These oscillations, while intriguing, are consistent with the model. With increasing size, ρ_c decreases (eq 14) and ρ/ρ_c increases, resulting in progressively higher and higher energy transitions (Δz = 1, 3, 5, ..., and so on) becoming a part of the collective resonance band. Each oscillatory maximum corresponds to the addition of the next Δz manifold to the collective resonance band.

Thus, the plasmon-in-a-box model, while simple, makes a number of interesting predictions that can be subject to experimental verification. The evolution of the plasmon resonance can be experimentally realized by controllably doping a semiconductor nanocrystal with increasing number of charge carriers. Such control has been shown to be possible. However, the spectral fine structure expected at a low number of carriers is unlikely to be observed at ambient temperatures due to phonon broadening of individual transitions. A low-temperature experiment would be needed. In addition, heterogeneous broadening of spectral lines due to nanocrystal-to-nanocrystal variations in size and/or doping level would further complicate the measurement, thus warranting a single-nanocrystal-level study, which is currently not without significant challenges. The increase in the width of the collective resonance band (Figure 1b) as it approaches the classical plasmon resonance is probably a more practically

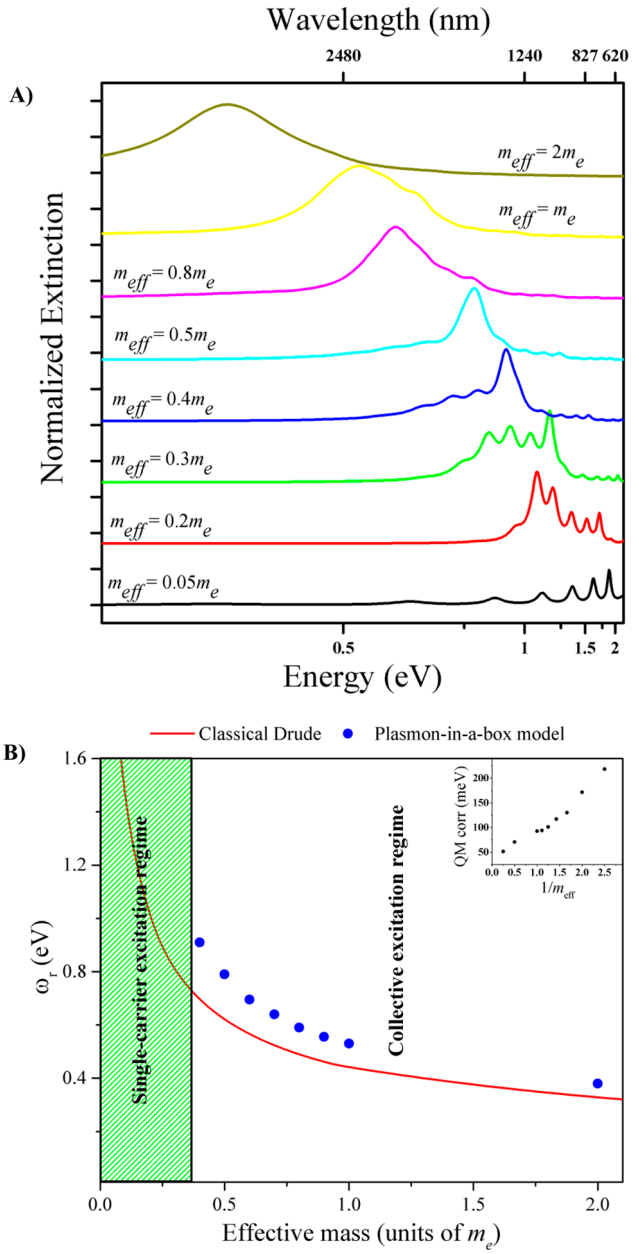

Figure 3. Effect of the bound nature of the carrier. (A) As the effective mass of the carrier increases, that is, the carrier becomes less bound or localized, a spectrum dominated by discrete quantum mechanical transitions evolves into one dominated by a collective excitation band. (B) Variation of the plasmon resonance frequency as a function of the effective mass, expressed in units of the free electron mass m_e of 9.1×10^{-31} kg. The calculated resonance frequency of the collective excitation band (blue) is higher than that obtained from a classical (Drude) free-carrier model (red curve). However, in the asymptotic limit of large effective mass, the classical plasmon resonance frequency is approached. (Inset) The deviation of the quantum mechanical result from the Drude model becomes smaller with increasing effective mass. Calculations for this figure were performed for an a = 8 nm nanocrystal with a carrier density of $\rho = 10^{27}$ m^{-3}. Values of other parameters were $\varepsilon_m = 2.1$, $\varepsilon_\infty = 3$, and $\gamma = 4\pi \times 10^{13}$ rad/s.

dx.doi.org/10.1021/jz501456t | J. Phys. Chem. Lett. 2014, 5, 3112−3119

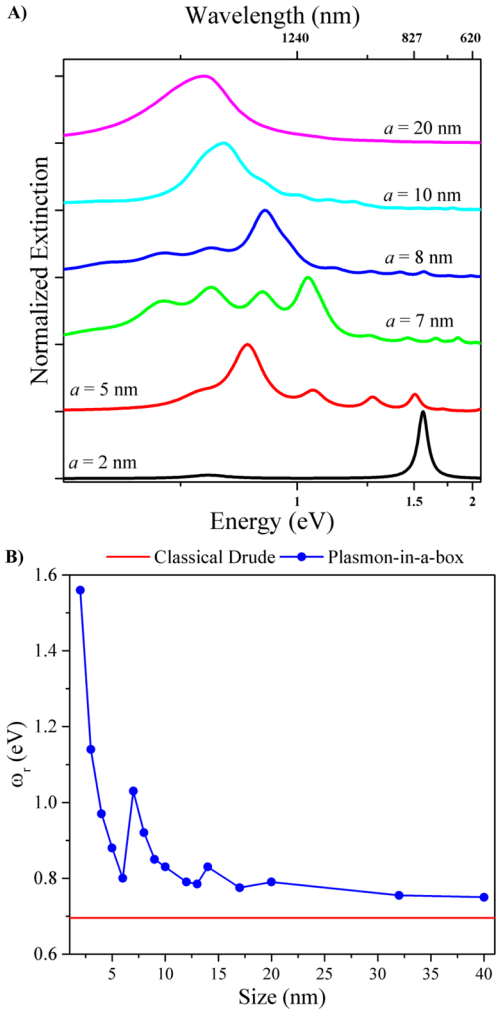

Figure 4. Effect of nanocrystal size. (A) As the size of the nanocrystal increases, that is, carriers become less confined, a spectrum dominated by discrete quantum mechanical transitions evolves into one dominated by a collective excitation band. (B) The calculated resonance frequency of the strongest transition (blue) is seen to undergo oscillations with size as it approaches, in the limit of large size, the classical plasmon resonance frequency obtained from the Drude model (red line). Calculations for this figure were performed for a carrier density of $N = 10^{27}$ m^{-3}. Values of other parameters were $m_{eff} = 0.4m_e$, $\varepsilon_m = 2.1$, $\varepsilon_\infty = 3$, and $\gamma = 4\pi \times 10^{13}$ rad/s.

realizable prediction. In addition, the oscillation in the resonance frequency as a function of increasing size is also worth exploring, provided that the carrier density can be held constant across different nanocrystal sizes.

The following insights are offered by the theoretical results presented here:

(a) At very low carrier densities, intraband transitions of single carriers between quantum mechanical levels dominate the optical response. Collective excitations are unimportant.

(b) A charge carrier collection begins to exhibit collective excitations when the carrier density ρ surpasses a critical density ρ_c At this critical density, Coulomb interactions between carriers begin to overcome the confinement of Fermi level carriers to the lattice.

(c) The classical plasmon resonance, characteristic of electron-dense metals, is approached only when $\rho \gg \rho_c$, at which point, all carriers within the sea participate in a collective excitation. Until this high density limit is reached, there exists a rather extended intermediate density regime ($\rho > \rho_c$), wherein both quantum mechanical single-carrier excitations and few-carrier collective excitations coexist. In this intermediate regime, the number of correlated carriers that characterize a collective excitation increases with increasing ρ/ρ_c.

(d) The more bound the carriers, the higher the critical density ρ_c required for collective excitations to be exhibited. On a similar note, the smaller the size of the nanocrystal, the higher the critical density ρ_c.

(e) The emergence of a plasmon resonance is thus a density-driven transition. This transition is a gradual one, quite unlike the well-known Mott insulator-to-metal transition, which is a sharp transition.

Semiconductor nanocrystals are ideal model systems for accessing the intermediate carrier density regime and probing, in depth, the nature of the transition. A good example is the recently reported plasmon-resonance-like absorption in 3 nm size ZnO nanocrystals photodoped with few electrons.[19] Taking into account the effective mass of $0.24m_e$ for these electrons, ρ_c for this case is calculated to be 2×10^{23} m^{-3}. In comparison, the carrier density ρ, based on the estimated four photoelectrons added to the ZnO conduction band, is 4×10^{26} m^{-3}. Thus, ρ is significantly larger than ρ_c but not as large as that in a metal (ca. 10^{29} m^{-3}).

Further theory is needed to elucidate the characteristic number of carriers involved in a collective excitation and also the nature of carrier−carrier interactions as a function of ρ/ρ_c. More rigorous treatments through ab initio[37] and molecular dynamics methods[38] like quantum Monte Carlo would shed light on this topic, especially by inclusion of electron−electron correlations and realistic effects such as temperature-dependent phonon scattering. Insight from the present and future work can be useful for the realization of nanocrystal-based optoelectronic devices where dynamic manipulation of light relies on active carrier doping.[11] Understanding of the energy level structure and excited-state behavior of charge carrier collections in molecular-size semiconductor and metal clusters is also relevant in photoelectrolytic applications.[39,40]

METHODS SECTION

Carriers added to the empty free-carrier band of a nanocrystal are assumed to be confined to a three-dimensional cubic box of side a. The allowed energy levels within the free-carrier band are given by

$$E_{x,y,z} = \frac{h^2(x^2 + y^2 + z^2)}{8m_{eff}a^2} \quad \text{(M1)}$$

where h is Planck's constant, x, y, and z are quantum numbers, and m_{eff} is the effective mass of the carrier. For n carriers added to this nanocrystal, $n/2$ levels are filled, and the Fermi energy is given by

$$E_F = \frac{h^2 z_F^2}{8m_{eff}a^2} \quad \text{(M2)}$$

where z_F is the intersection of the z-axis with the surface of the three-dimensional Fermi sphere, given by

$$z_F = \left(\frac{3n}{\pi}\right)^{1/3} \approx n^{1/3} \quad \text{(M3)}$$

Note that spin degeneracy is included by allowing two charge carriers to occupy each allowed level.

dx.doi.org/10.1021/jz501456t | J. Phys. Chem. Lett. 2014, 5, 3112−3119

Description of the Dielectric Function. The optical response of carriers confined to this box is given by its dielectric function[32,34]

$$\varepsilon(\omega) = \varepsilon_{ib}(\omega) + \frac{e^2}{\varepsilon_0 m_{\text{eff}} a^3} \sum_{\text{i,f}} \frac{A_{\text{i,f}}}{\omega_{\text{i,f}}^2 - (\omega^2 + \text{i}\omega\gamma_{\text{i,f}})} \tag{M4}$$

Here, the second term represents the dielectric polarization per unit volume obtained by taking into account all possible transitions between discrete energy levels of the nanocrystal. ε_0 is the permittivity of free space. $\varepsilon_{\text{ib}}(\omega)$ is the dielectric function resulting from interband transitions. Because intricate details of band structure and band-to-band transitions are not germane to the discussion here, the author approximates $\varepsilon_{\text{ib}}(\omega)$ by a high-frequency dielectric constant ε_∞, which has satisfactorily reproduced experimental data in a number of cases. Relativistic effects are ignored here.

The i represents the initial state involved in the transition with a quantum number z, and f represents the final state with the quantum number $z + \Delta z$. $\gamma_{\text{i,f}}$ is the damping frequency of the transition, and $\omega_{\text{i,f}}$ is the transition frequency given by

$$\omega_{\text{i,f}} = \omega_{z,\Delta z} = 2\pi \frac{\Delta E_{\text{i,f}}}{h} = 2\pi \Delta z(2z + \Delta z) \frac{h}{8 m_{\text{eff}} a^2} \tag{M5}$$

and the oscillator strength $A_{\text{i,f}}$ of the transition is given by Kreibig[34] as

$$A_{\text{i,f}} = A_{z,\Delta z} = \frac{64}{\pi^2} \frac{z^2(z + \Delta z)^2}{\Delta z^3 (2z + \Delta z)^3} \delta_{x_i,x_f} \delta_{y_i,y_f} \tag{M6}$$

The broadening of the Fermi–Dirac distribution is also ignored; the initial state is below the Fermi level, and the final state is above the Fermi level. The incident light polarization is assumed to be along the z-direction; therefore, only transitions along the z-direction given by $\delta_{x_i,x_f} = \delta_{y_i,y_f} = 1$ are considered. Thus, we take advantage of the isotropic shape. More complex nanocrystal shapes can lift the symmetry and influence the observed optical response (e.g., introduce anisotropy), but this is outside of the scope of the work here. Also, it must be noted that for optically allowed transitions, Δz is an odd integer. The summation in eq M4 over all possible transitions can be further simplified by combining all degenerate transitions of a given z and Δz as

$$\varepsilon(\omega) = \varepsilon_\infty + \frac{e^2}{\varepsilon_0 m_{\text{eff}} a^3} \sum_{\Delta z}^{1,3,\ldots} \sum_{z}^{1,2,\ldots,z_F} \frac{A_{z,\Delta z} \Omega_{z,\Delta z}}{\omega_{z,\Delta z}^2 - (\omega^2 + \text{i}\omega\gamma_{z,\Delta z})} \tag{M7}$$

where the degeneracy factor $\Omega_{z,\Delta z}$ including a spin degeneracy of 2 is given as

$$\Omega_{z,\Delta z} = \frac{\pi}{2}(2z + \Delta z) \cdot \Delta z \tag{M8}$$

Assumptions in the Model. The author acknowledges that such an effective mass model provides only an approximate description of the electronic response of the doped semiconductor nanocrystal. It must be noted that for very small and very large nanocrystals, the effective mass approximation may not be completely reliable.[41] In addition, transitions involving higher-lying energy levels cannot be treated in a parabolic approximation. For a more accurate treatment of carriers in the valence band of typical semiconductors, contributions from light holes, heavy holes, and split-off bands must be included.

The author also assumes that the electronic band structure is not influenced by the addition of charge carriers to the empty band or by variations in the crystallite size. No electron–electron exchange correlations are included. Finite-temperature effects such as phonon broadening are ignored, although $\gamma_{\text{i,f}}$ can be increased to phenomenologically study the effect of such broadening. For simplicity, the same value of $\gamma_{\text{i,f}}$ is used for all intraband transitions regardless of the states involved in the transition. In practice, each intraband transition can have a unique lifetime $(1/\gamma_{\text{i,f}})$, which is a possible physical origin for the recent observation of a frequency-dependent damping constant for the plasmon resonance of doped semiconducting oxide nanocrystals.[42]

Calculation of the Optical Extinction Spectrum. In the quasistatic electric-dipole approximation (valid for nanocrystal sizes much smaller than the wavelength of light), the optical polarizability of the nanocrystal is given by the Clausius–Mossotti relation as

$$\alpha(\omega) = 3a^3 \frac{(\varepsilon(\omega) - \varepsilon_{\text{m}})}{(\varepsilon(\omega) + \kappa\varepsilon_{\text{m}})} \tag{M9}$$

where ε_{m} is the dielectric constant of the medium. A cubic shape does not have an analytic value for κ (although it is estimated to be ca. 3 in the dipolar limit); the author uses $\kappa = 2$, the analytic value for a spherical shape, which is not expected to change the physical meaning of the results.

The extinction cross section, $C(\omega)$ with units of m^2, is given as

$$C(\omega) = \frac{\omega}{c} \varepsilon_{\text{m}}^{1/2} \,\text{Im}(\alpha(\omega)) \tag{M10}$$

For the summation in eq M7, the upper limit of Δz was set to be 100, which was verified to be sufficient for convergence of the series.

■ ASSOCIATED CONTENT

Supporting Information

Comparison of calculated spectra to experimental plasmon resonance spectra for a Au nanosphere and a doped $Cu_{2-x}Se$ (x = 0.2) nanocrystal. This material is available free of charge via the Internet at http://pubs.acs.org.

■ AUTHOR INFORMATION

Corresponding Author

*E-mail: jain@illinois.edu.

Notes

The authors declare no competing financial interest.

■ ACKNOWLEDGMENTS

The work of P.K.J. was funded through the Sloan Research Fellowship from the Alfred P. Sloan Foundation.

■ REFERENCES

(1) Link, S.; El-Sayed, M. A. Size and Temperature Dependence of the Plasmon Absorption of Colloidal Gold Nanoparticles. *J. Phys. Chem. B* **1999**, *103*, 4212–4217.

(2) Wang, H.; Brandl, D. W.; Nordlander, P.; Halas, N. J. Plasmonic Nanostructures: Artificial Molecules. *Acc. Chem. Res.* **2007**, *40*, 53–62.

(3) Sardar, R.; Funston, A. M.; Mulvaney, P.; Murray, R. W. Gold Nanoparticles: Past, Present, And Future. *Langmuir* **2009**, *25*, 13840–13851.

(4) Ringe, E.; McMahon, J. M.; Sohn, K.; Cobley, C.; Xia, Y.; Huang, J.; Schatz, G. C.; Marks, L. D.; Van Duyne, R. P. Unraveling the Effects of Size, Composition, and Substrate on the Localized Surface Plasmon Resonance Frequency of Gold and Silver Nanocubes: A Systematic Single Particle Approach. *J. Phys. Chem. C* **2010**, *114*, 12511−12516.
(5) Haberland, H.; von Issendorff, B.; Yufeng, J.; Kolar, T. Transition to Plasmonlike Absorption in Small Hg Clusters. *Phys. Rev. Lett.* **1992**, *69*, 3212−3215.
(6) Kreibig, U.; Genzel, L. Optical Absorption of Small Metallic Particles. *Surf. Sci.* **1985**, *156*, 678−700.
(7) Desireddy, A.; Conn, B. E.; Guo, J.; Yoon, B.; Barnett, R. N.; Monahan, B. M.; Kirschbaum, K.; Griffith, W. P.; Whetten, R. L.; Landman, U.; Bigioni, T. P. Ultrastable Silver Nanoparticles. *Nature* **2013**, *501*, 399−402.
(8) Faraday, M. The Bakerian Lecture: Experimental Relations of Gold (and Other Metals) to Light. *Philos. Trans. R. Soc.* **1857**, *147*, 145−181.
(9) Zhao, Y.; Pan, H.; Lou, Y.; Qiu, X.; Zhu, J.; Burda, C. Plasmonic $Cu_{(2-x)}S$ Nanocrystals: Optical and Structural Properties of Copper-Deficient Copper(I) Sulfides. *J. Am. Chem. Soc.* **2009**, *131*, 4253−4261.
(10) Luther, J. M.; Jain, P. K.; Ewers, T.; Alivisatos, A. P. Localized Surface Plasmon Resonances Arising from Free Carriers in Doped Quantum Dots. *Nat. Mater.* **2011**, *10*, 361−366.
(11) Routzahn, A. L.; White, S. L.; Fong, L.-K.; Jain, P. K. Plasmonics with Doped Quantum Dots. *Isr. J. Chem.* **2012**, *52*, 983−991.
(12) Dorfs, D.; Härtling, T.; Miszta, K.; Bigall, N. C.; Kim, M. R.; Genovese, A.; Falqui, A.; Povia, M.; Manna, L. Reversible Tunability of the Near-Infrared Valence Band Plasmon Resonance in $Cu_{(2-x)}Se$ Nanocrystals. *J. Am. Chem. Soc.* **2011**, *133*, 11175−11180.
(13) Della Valle, G.; Scotognella, F.; Ram, A.; Kandada, S.; Zavelani-rossi, M.; Li, H.; Conforti, M.; Longhi, S.; Manna, L.; Lanzani, G.; et al. Ultrafast Optical Mapping of Nonlinear Plasmon Dynamics in $Cu_{2-x}Se$ Nanoparticles. *J. Phys. Chem. Lett.* **2013**, *4*, 3337−3344.
(14) Manthiram, K.; Alivisatos, A. P. Tunable Localized Surface Plasmon Resonances in Tungsten Oxide Nanocrystals. *J. Am. Chem. Soc.* **2012**, *134*, 3995−3998.
(15) Garcia, G.; Buonsanti, R.; Runnerstrom, E. L.; Mendelsberg, R. J.; Llordes, A.; Anders, A.; Richardson, T. J.; Milliron, D. J. Dynamically Modulating the Surface Plasmon Resonance of Doped Semiconductor Nanocrystals. *Nano Lett.* **2011**, *11*, 4415−4420.
(16) Kriegel, I.; Rodríguez-Fernández, J.; Wisnet, A.; Zhang, H.; Waurisch, C.; Eychmüller, A.; Dubavik, A.; Govorov, A. O.; Feldmann, J. Shedding Light on Vacancy-Doped Copper Chalcogenides: Shape-Controlled Synthesis, Optical Properties, and Modeling of Copper Telluride Nanocrystals with Near-Infrared Plasmon Resonances. *ACS Nano* **2013**, *7*, 4367−4377.
(17) Yang, H.; Chen, C.; Yuan, F.; Tuan, H. Designed Synthesis of Solid and Hollow $Cu_{2-x}Te$ Nanocrystals with Tunable Near-Infrared Localized Surface Plasmon Resonance. *J. Phys. Chem. C* **2013**, *117*, 21955−21964.
(18) Polking, M. J.; Jain, P. K.; Bekenstein, Y.; Banin, U.; Millo, O.; Ramesh, R.; Alivisatos, A. P. Controlling Localized Surface Plasmon Resonances in GeTe Nanoparticles Using an Amorphous-to-Crystalline Phase Transition. *Phys. Rev. Lett.* **2013**, *111*, 037401.
(19) Faucheaux, J. A.; Jain, P. K. Plasmons in Photocharged ZnO Nanocrystals Revealing the Nature of Charge Dynamics. *J. Phys. Chem. Lett.* **2013**, *4*, 3024−3030.
(20) Buonsanti, R.; Llordes, A.; Aloni, S.; Helms, B. A.; Milliron, D. J. Tunable Infrared Absorption and Visible Transparency of Colloidal Aluminum-Doped Zinc Oxide Nanocrystals. *Nano Lett.* **2011**, *11*, 4706−4710.
(21) Schimpf, A. M.; Thakkar, N.; Gunthardt, C. E.; Masiello, D. J.; Gamelin, D. R. Charge-Tunable Quantum Plasmons in Colloidal Semiconductor Nanocrystals. *ACS Nano* **2014**, *8*, 1065−1072.
(22) Faucheaux, J. A.; Stanton, A. L. D.; Jain, P. K. Plasmon Resonances of Semiconductor Nanocrystals: Physical Principles and New Opportunities. *J. Phys. Chem. Lett.* **2014**, *5*, 976−985.
(23) Shim, M.; Guyot-Sionnest, P. Organic-Capped ZnO Nanocrystals: Synthesis and n-Type Character. *J. Am. Chem. Soc.* **2001**, *123*, 11651−11654.
(24) Bohm, D.; Pines, D. A Collective Description of Electron Interactions: III. Coulomb Interactions in a Degenerate Electron Gas. *Phys. Rev.* **1953**, *92*, 609−625.
(25) Selby, K.; Vollmer, M.; Masui, J.; Kresin, V.; de Heer, W. A.; Knight, W. D. Surface Plasma Resonances in Free Metal Clusters. *Phys. Rev. B* **1989**, *40*, 5417.
(26) Rademann, K.; Dimopoulou-Rademann, O.; Schlauf, M.; Even, U.; Hensel, F. Evolution of Surface Plasmon Resonance Absorption in Large Gas Phase Clusters of Mercury: Approaching the Bulk. *Phys. Rev. Lett.* **1992**, *69*, 3208.
(27) Zhu, M.; Aikens, C. M.; Hollander, F. J.; Schatz, G. C.; Jin, R. Correlating the Crystal Structure of a Thiol-Protected Au_{25} Cluster and Optical Properties. *J. Am. Chem. Soc.* **2008**, *130*, 5883−5885.
(28) Townsend, E.; Bryant, G. W. Plasmonic Properties of Metallic Nanoparticles: The Effects of Size Quantization. *Nano Lett.* **2012**, *12*, 429−434.
(29) Jain, P. K.; Manthiram, K.; Engel, J. H.; White, S. L.; Faucheaux, J. A.; Alivisatos, A. P. Doped Nanocrystals as Plasmonic Probes of Redox Chemistry. *Angew. Chem., Int. Ed.* **2013**, *52*, 13671−13675.
(30) Sahu, A.; Kang, M. S.; Kompch, A.; Notthoff, C.; Wills, A. W.; Deng, D.; Winterer, M.; Frisbie, C. D.; Norris, D. J. Electronic Impurity Doping in CdSe Nanocrystals. *Nano Lett.* **2012**, *12*, 2587−2594.
(31) Mocatta, D.; Cohen, G.; Schattner, J.; Millo, O.; Rabani, E.; Banin, U. Heavily Doped Semiconductor Nanocrystal Quantum Dots. *Science* **2011**, *332*, 77−81.
(32) Kraus, W. A.; Schatz, G. C. Plasmon Resonance Broadening in Small Metal Particles. *J. Chem. Phys.* **1983**, *79*, 6130−6139.
(33) Zhang, H.; Kulkarni, V.; Prodan, E.; Nordlander, P.; Govorov, A. O. Theory of Quantum Plasmon Resonances in Doped Semiconductor Nanocrystals. *J. Phys. Chem. C* **2014**, *118*, 16035−16042.
(34) Genzel, L.; Martin, T. P.; Kreibig, U. Dielectric Function and Plasma Resonances of Small Metal Particles. *Z. Phys. B* **1975**, *21*, 339−346.
(35) Scholl, J. A.; Koh, A. L.; Dionne, J. A. Quantum Plasmon Resonances of Individual Metallic Nanoparticles. *Nature* **2012**, *483*, 421−427.
(36) Haberland, H. Looking from Both Sides. *Nature* **2013**, *494*, E1−2.
(37) Wang, L. G.; Zunger, A. Cluster-Doping Approach for Wide-Gap Semiconductors: the Case of p-Type ZnO. *Phys. Rev. Lett.* **2003**, *90*, 256401.
(38) Ren, J.; Vukmirović, N.; Wang, L.-W. Nonadiabatic Molecular Dynamics Simulation for Carrier Transport in a Pentathiophene Butyric Acid Monolayer. *Phys. Rev. B* **2013**, *87*, 205117.
(39) Chen, Y. S.; Choi, H.; Kamat, P. V. Metal-Cluster-Sensitized Solar Cells. A New Class of Thiolated Gold Sensitizers Delivering Efficiency Greater than 2%. *J. Am. Chem. Soc.* **2013**, *135*, 8822−8825.
(40) Hartland, G. V. Assembling Atoms to Clusters and Clusters to Crystals. *J. Phys. Chem. Lett.* **2011**, *2*, 1111−1112.
(41) Norris, D. J.; Bawendi, M. G. Measurement and Assignment of the Size-Dependent Optical Spectrum in CdSe Quantum Dots. *Phys. Rev. B* **1996**, *53*, 16338−16346.
(42) Mendelsberg, R. J.; Garcia, G.; Li, H.; Manna, L.; Milliron, D. J. Understanding the Plasmon Resonance in Ensembles of Degenerately Doped Semiconductor Nanocrystals. *J. Phys. Chem. C* **2012**, *116*, 12226−12231.